Inorganica Chimica Acta 514 (2021) 120025

Contents lists available at ScienceDirect

Inorganica Chimica Acta

journal homepage: www.elsevier.com/locate/ica

Research paper

New fast synthesis of MOF-801 for water and hydrogen storage: Modulator effect and recycling options

Vera V. Butova, Ilia A. Pankin, Olga A. Burachevskaya, Kristina S. Vetlitsyna-Novikova, Alexander V. Soldatov

The Smart Materials Research Institute, Southern Federal University, Sladkova Str. 178/24, Rostov-on-Don 344090, Russia

ARTICLE INFO

Keywords:
Metal-organic frameworks
MOF
Modulator
Acetic acid
Zirconium fumarate

ABSTRACT

We report a new simple, fast, scalable technique for MOF-801 synthesis. The effect of modulators on crystallinity, size, and shape of particles, porosity, hydrogen and water uptake was traced using two mono-carboxylic acids with various concentrations. We also showed that slow heating and small grains in powder samples are optimal for fast water release at relatively low temperatures. Heating up to 60–80 °C is enough for complete water release in 40 min, while at 40 °C, after 100 min, water is retained in pores of the sorbent. It was shown that both acetic and formic acids enhance the properties of MOF-801 material. However, even without any additives, proposed synthesis conditions lead to porous, highly crystalline material with hydrogen uptake about 1.1 wt% at 750 mmHg and water uptake about 20% at ambient conditions. We proved that solvent from the synthesis of MOF-801 could be used at least four times without any degradation of the obtained sorbent in key properties.

1. Introduction

Metal-organic frameworks (MOFs) are porous materials that attract a lot of attention recently [1]. According to the concept of reticular chemistry, MOFs could be constructed from two counterparts – secondary building units (SBUs) and linkers [2]. SBUs are inorganic clusters, which contain one or more metal ions coordinated by oxygen or nitrogen. These clusters are bonded to each other through organic molecules – linkers. Numerous possible combinations of SBUs and linkers result in a great number of MOFs.

Moreover, particular MOF could be additionally tuned toward the desired application by the introduction of functional groups to linkers. This flexibility of MOFs leads to their success in various fields such as gas storage and separation [3], catalysis [4–5], water and air purification [6–7], biomedicine [8–9], and others. However, not only the composition and crystal structure of MOFs is crucial for most applications. The size of particles and the concentration of defects could have a significant impact on the properties of resulting materials. The concept of coordination modulation could be used for intelligent control of morphology and size of particles, defects, and crystallinity of MOFs [10]. According to this concept introduction of mono-carboxylic acids into the reaction mixture during the synthesis of MOFs results in modulation of the crystallization process. Mono-carboxylic acids, in this way, act as modulators. They compete with linkers for the coordination of metal ions. As the concentration of modulators is usually higher than the concentration of linker molecules, at the first moment, metal ions build the coordination spheres from modulator molecules. However, the linker could form more than one bond with metal ions, and it substitutes modulators during the reaction process. It results in slower crystal growth and higher crystallinity of obtained MOFs. A very high concentration of modulators could result in defect formation when substitution of modulators is slower than crystal growth.

The present investigation is focused on MOF-801. It is constructed from Zr-SBUs and fumarate linkers. Each SBU contains six Zr ions. Each ion is coordinated by eight oxygen ions – 4 from the carboxylic groups of fumarate linkers and four bridge oxygen ions. Each SBU is coordinated by 12 linkers (Fig. S1). Strong covalent bonds and high coordination of SBUs result in a very stable framework. MOF-801 contains three types of pores – two tetrahedral and octahedral. Fumarate ions are not linear, and carboxylic groups are located not exactly under each other but shifted from the line of double-bond in opposite directions (Fig. S1a). It leads to slightly tilted SBUs and two types of tetrahedral pores – 5.6 Å and 4.8 Å. Octahedral pores have a diameter of about 7.4 Å. Such small pores are optimal for the adsorption of small molecules. MOF-801 was applied for hydrogen [11–12] and water storage [13–18], removal of fluoride [19–21], arsenide [22] and chromium [23–24] ions. For MOF-801 synthesis, various methods were used (Table S1). It was reported that MOF-801 could be obtained in water solution by heating reaction mixture at 120 °C for 24 h with modulator additives [20,25–26]. Most parts of the reported procedures include

E-mail address: vbutova@sfedu.ru (A.V. Soldatov).

https://doi.org/10.1016/j.ica.2020.120025
Received 15 August 2020; Received in revised form 15 September 2020; Accepted 15 September 2020
Available online 19 September 2020
0020-1693/

synthesis in DMF solution due to it provides higher solubility of precursors and do not initiate hydrolysis of zirconium salt [12–13,15–16,18–19,21–24,27–31]. Authors use modulator additives and/or linker excess to increase the yield of reaction and to enhance the porosity of the product. However, these features obstruct the re-use of solvent after synthesis, while recycling of DMF could reduce the environmental impact and cost of the product.

In the present work, we have optimized the solvothermal synthesis of MOF-801 in DMF. We applied both modulated and non-modulated routes to prove that fast synthesis without modulator or excess of linker does not degrade such key properties of MOF-801 as hydrogen and water capacities.

2. Experimental

2.1. Synthesis

Starting materials zirconium tetrachloride ($ZrCl_4$), fumaric acid (H_2FC), acetic acid (AA), formic acid (FA), N, *N*-dimethylformamide (DMF), methanol were purchased from commercial suppliers and used without further purification. Deionized (DI) water (18 MΩcm) was obtained from a Simplicity UV ultrapure water system.

In a typical procedure, $ZrCl_4$ was dissolved in DMF under magnetic stirring, then DI water was added. After that, the respective amount of AA/FA was added, and after complete dissolving, H_2FC was poured to the clear solution (Table 1). The conical flask was capped and place into the preheated oven at 120 °C for two hours. After cooling to room temperature, white precipitates were collected using centrifugation, washed two times with DMF and one time with methanol, and dried at 60 °C overnight.

2.2. Recycling

Synthesis MOF-801 was reproduced according to the procedure mentioned above. Briefly, 0.2008 g of $ZrCl_4$ was dissolved in 20 ml of DMF under magnetic stirring. After this, 46.6 μl of DI water was added. Finally, 0.1000 g of H_2FC was admixed to the clear solution. The reaction mixture in a closed glass vessel was placed into a preheated oven for two hours at 120 °C. After cooling down, the precipitate was collected by centrifugation and treated as previously obtained samples. Separated DMF was used for the second synthesis. We applied four cycles with the same solvent. Each precipitate was denoted as MOF-801 with a number of cycles. For example, sample MOF-801–1 was synthesized in new DMF, while for the synthesis of the sample MOF-801–3, we used DMF after two cycles, so it was the third synthesis in the same DMF.

2.3. Characterization methods

Powder X-ray diffraction (PXRD) was measured on a Bruker D2 PHASER X-ray diffractometer (CuKα, λ = 1.5417 Å) with a step of 0.01°. The full profile PXRD analysis was performed by using MAUD software [32–33]. Prior to the refinement for the samples investigated in this work, the experimental function was derived by using the PXRD pattern of Al_2O_3 standard (corundum) free from the effect of small crystallite size broadening and lattice defects. The experimental function was approximated by using the Caglioti polynomial function parametrized by few parameters accounting for peaks width and asymmetry.

For all the samples, the goodness of the fit (GoF) was estimated as $\chi = \sqrt{\frac{R_{wp}^2}{R_{exp}^2}}$ [34]. The PXRD refinement for the standard Al_2O_3 was performed for the PXRD pattern in the range from 20° to 70° in 2θ. Conversely, for the analysis of MOF-801 samples, the 2θ range from 2° to 55° has been employed for full profile analysis. As an initial guess for the PXRD fit, the structure of MOF-801, as reported by H. Furukawa and co-workers [13] has been utilized. In our work, full profile analysis has been parameterized by the background coefficients and few structural parameters such as lattice parameter *a*, an average crystalline size < D > within an isotropic model, and microstrains ε. At the same time, positions and occupancies of different atomic sites have not been refined. The results of the full profile analysis are summarized in Table 2. A high-resolution transmission electron microscope (HTEM) FEI Tecnai G2 F20 was employed for the imaging of the samples. IR spectra were measured on a Bruker Vertex 70 spectrometer in ATR (Attenuated total reflectance) geometry using an MCT detector and a Bruker Platinum ATR attachment. The spectra were measured in the range from 5000 to 300 cm^{-1} with a resolution of 1 cm^{-1} and 128 scans. The reference is air. The specific surface area (BET) values and hydrogen capacities of the samples were determined from nitrogen (hydrogen) adsorption/desorption isotherms at −196 °C obtained on Accelerated Surface Area and Porosimetry analyzer ASAP 2020 (Micromeritics). The samples were activated at 150 °C for 10 h under a dynamic vacuum before the measurement. Thermogravimetric analysis (TGA) was performed on the thermal gravimetric analyzer STA 449 F5 Jupiter with a low drift balance. Samples in corundum crucibles were heated with a rate of 5–10°/min in the flux of air or nitrogen.

Table 1
Molar ratio of precursors used for the synthesis of MOF-801 samples.

Sample designation	The molar ratio of components used for the synthesis					
	$ZrCl_4$	H_2FC	H_2O	AA	FA	DMF
MOF-801	1	1	3	–	–	300
MOF-801-10AA				10	–	
MOF-801-10FA				–	10	
MOF-801-30AA				30	–	
MOF-801-30FA				–	30	

3. Results and discussion

3.1. Effect of modulators

According to powder XRD, all obtained samples have the same structure in good agreement with previously reported data for MOF-801 (Fig. 1a). All reflections could be assigned to cubic symmetry, space group *Pn*-3 (201). We have not observed any specific trend in the evolution of the lattice parameters. Only MOF-801–10-AA demonstrates a slightly elongated lattice parameter *a* with respect to all other samples. However, it is clearly demonstrated that an averaged crystallite size < D > increases with the increase of modulator loading. It should also be mentioned that the sample obtained without modulators (MOF-801) also demonstrates a high level of crystallinity reflected in an averaged crystallite size < D > equal to 30.5 nm, and very low values obtained for microstrains ε (Table 2). FTIR spectra of obtained samples are presented in Fig. 1b. For all samples, they are quite similar and are in good agreement with previously reported data for zirconium MOFs. The first two peaks at 490 and 660 cm^{-1} could be attributed to Zr-(OC) asymmetric stretching and the vibration of the $Zr_6(OH)_4O_4$ cluster, respectively [35]. Modes at 795 cm^{-1}, 990 cm^{-1} and 1210 cm^{-1} could be assigned to C—H vibrations [35–36]. Absorption at 1400 cm^{-1} is attributed to the O—C—O symmetric stretching in a carboxylic group of a linker, while asymmetric stretching of this group gives rise to bands at 1650 cm^{-1} and 1570 cm^{-1} [35,37].

The morphology of synthesized particles and the effect of modulators were traced using TEM (Fig. 2, Fig. S2). It was observed that modulator additive increases the size of particles in good agreement with previously reported data [38–39] (Table 2, Fig. 2). The morphology of obtained crystals could be assigned to cubic with smoothed edges in good agreement with reported data [19].

TGA curves in airflow for all obtained samples are provided in

Table 2
Some properties of synthesized samples. SSA stands for specific surface area.

Sample designation	Profile analysis				SSA, m^2/g	Pore volume, cm^3/g	H_2 capacity, wt.%	
	a, Å	Micro-strains ε	Particle size < D >, nm	GOF			20 mmHg	750 mmHg
MOF-801	17.915	$9.37\ 10^{-8}$	30.53	1.23	595	0.27	0.228	1.107
MOF-801-10AA	17.930	$1.06\ 10^{-6}$	27.19	1.45	578	0.28	0.216	1.034
MOF-801-10FA	17.918	$1.37\ 10^{-6}$	23.63	1.43	556	0.29	0.210	1.005
MOF-801-30AA	17.910	$1.14\ 10^{-3}$	34.47	1.22	632	0.31	0.222	1.070
MOF-801-30FA	17.913	$4.44\ 10^{-4}$	35.02	1.56	632	0.31	0.229	1.131

(Fig. 3a). They were rescaled according to the method proposed by Loredana Valenzano and coauthors for UiO-66 [40]. The residual after heating of MOF-801in the airflow is zirconium oxide. Six mols of ZrO_2 could be obtained from one formula unit of MOF-801.

$$Zr_6O_4(OH)_4(C_4O_4H_2)_6 + 18O_2 = 6ZrO_2 + 24CO_2 + 8H_2O \quad (1)$$

The weight of 6 mols of ZrO_2 was used as 100%. We have calculated the theoretical position of the plateau according to the stoichiometry of MOF-801 (dashed lines in Fig. 3a). Theoretical weight loss is 37%, according to $Zr_6O_4(OH)_4(C_4O_4H_2)_6$ stoichiometry. All samples demonstrate similar shapes of TGA curves and weight loss close to theoretical. Sample MOF-801-10AA slightly deviates from other samples and demonstrates 43% weight loss. DSC curves of all samples contain three picks. The first one at 83 °C is negative, which corresponds to the endothermic process of evacuation of water molecules from the pores. The second process is exothermic, and pick at 400 °C could be attributed to the breaking of the coordinated bonds between the fumarate-linkers and SBUs. It results in the formation of ZrO_2 particles with a graphitized carbon shell [41]. The last pick at 590 °C also corresponds to the exothermic process. It could be assigned to the decomposition of carbon shells and the formation of pure ZrO_2 as a final solid product of the reaction (1). Considering high research interest on MOF-801 application for water harvesting [13,15–16,42] we have thoroughly investigated water adsorption/desorption properties of the synthesized materials via the TGA experiment under a controlled atmosphere. TGA has been collected in the inert flow of nitrogen (total flow of 50 ml/min) in the temperature range 25–160 °C (Fig. 3b). Before the measurements, all samples were treated in the same way. Firstly, they were dried at 60 °C for 24 h. Such relatively low temperature could not be sufficient to complete evacuation of all water molecules from MOF-801 (as it will be shown later). Still, it is relevant for the desorption cycle of water harvesting devices operating in the day/night mode earlier described in the literature [15–16]. After the activation, samples were left in the open space under room conditions (relative humidity (RH), about 48% and T = 25 °C; both relative humidity and temperature were fluctuating during the day, and an averaged value are reported herein) for 24 h. We suppose that after this treatment, samples were saturated with water, and we could estimate water capacity according to TGA. As it could be observed, the modulator does not significantly affect water capacity, and its values for all samples are in the range of 18.6–21.3%.

Samples start water desorption from the very beginning of heating at about 30 °C, and curves reached the plateau at about 120 °C. The rate of heating affects the water desorption process as well. According to TGA data, a slow heating rate 5 °C/min allows to get significantly faster weight loss with respect to the data measured with a heating rate 10° C/min, yielding the difference of *ca.* 2.8 wt% at 80° C (Fig. 4a). It proves that slow heating (for example, by the sun) will additionally shift the temperature of complete water desorption to relatively low temperatures. To prove this hypothesis, we have measured the weight loss of the sample MOF-801-10AA in isothermal conditions. Fig. 4b shows TGA isotherms measured for 40 °C, 60 °C, and 80 °C for the MOF801-10AA sample. Before the measurement, samples were activated at 60 °C for 24 h and subsequently were exposed at room conditions with RH about 50% and temperature 25 °C. For the lower temperature isotherm, the almost linear trend of weight loss is observed starting from the temperature of 40° C. While for isotherms at 60° C and 80° C fast exponential weight loss is observed. In both cases, fast exponential weight loss is followed by the linear trend with an almost similar slope. After 40 min of heating samples at 60 °C and 80 °C have lost 20% of the weight and reached the plateau. Obviously, the curvature of the exponential range of the TGA curve is stronger for 80 °C isotherm. More interesting that there is a constant difference of *ca.* 2 wt% in the linear part of 60 °C and 80 °C isotherms. It clearly shows that some portion of water molecules is still not accessible at 60 °C, even in the case of prolonged heating. These results of particular interest because in the water harvesting applications, the temperature of the MOF-based

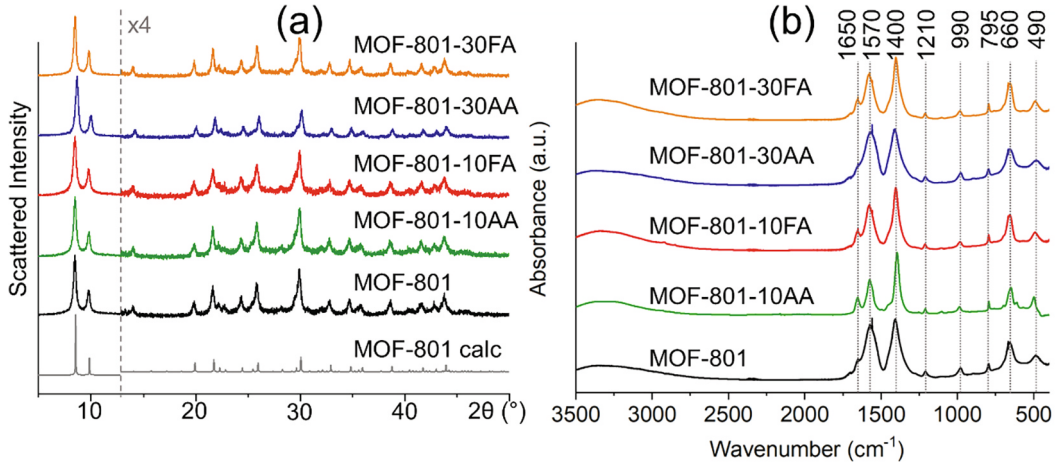

Fig. 1. Powder XRD patterns (a) and FTIR-spectra (b) of synthesized MOF-801-samples. Patterns are shifted along the intensity-axis. In part (a) intensities were multiplied after dashed line for better representation. Profile MOF-801 calc was calculated according to crystallographic data [13]. In part (b) dotted lines highlight modes assigned to the MOF-801 structure (see text for details).

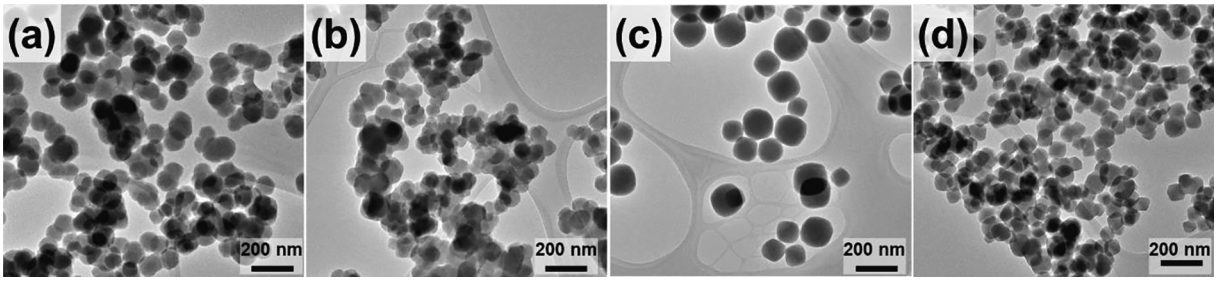

Fig. 2. TEM images of synthesized samples MOF-801-10AA (a), MOF-801-10FA (b), MOF-801-30AA (c), MOF-801-30FA (d).

absorber layer typically varies in range from 60 °C to 100 °C being heated by the solar energy upon the water desorption cycle. Another crucial point for fast water desorption is the size of particles in powder samples. Sample MOF-801 was sieved just after the activation by using μm sieves, and three fractions of the sample (with a grain size below 94 μm, 125 μm, and 250 μm) were held under room conditions for water uptake. Fig. 4c demonstrates TGA curves obtained for MOF-801 with different grain sizes. One can see that notable differences in the weight loss for the MOF-801 fractions with different particle sizes were obtained. Indeed, there is a clear trend in the range from 30 °C to 100 °C, which declares that a sample with a smaller particle more readily desorbs water molecules at a given temperature. This might be explained by the higher water adsorption capacity in the near-surface part of powder grains. Also, for sieved MOF-801 samples, slightly higher weight loss is observed at the temperature of 160 °C.

Nitrogen adsorption–desorption isotherms of synthesized samples are presented in Fig. 5. All of them could be assigned to type I, according to IUPAC classification. It indicates the microporous nature of materials. Nitrogen capacities of samples MOF-801, MOF-801-10AA, and MOF-801-10FA are rather close, while samples MOF-801-30AA and MOF-801-30FA exhibited slightly higher values. Specific surface areas, calculated according to the BET model, are in good agreement with nitrogen capacities (Table 2). For samples MOF-801, MOF-801-10AA, and MOF-801-10FA, they are in range 550–600 m^2/g, while for samples MOF-801-30AA and MOF-801-30FA, they were estimated as 632 m^2/g. All isotherms contain hysteresis loops of H1 type in IUPAC notification, which could be attributed to capillary condensation of nitrogen in slit-like cages between approximately uniform particles in agglomerates.

For hydrogen adsorption, we have observed a slightly different trend. All samples possess close hydrogen capacities both in the low-pressure region and at ambient pressure. Moreover, sample MOF-801 was synthesized without any modulators and exhibited one of the highest weight % of H_2. All isotherms showed a similar steep increase at the low-pressure range, and at ambient pressure, they did not reach saturation. Therefore, we suppose that at higher pressures, hydrogen capacity could be further increased.

3.2. Recycling of DMF

Fig. 6a represents powder XRD profiles of MOF-801 samples obtained during the recycling experiment. We did not observe any degradation of crystal structure even after the fourth synthesis in the same DMF. Moreover, from the preliminary visual examination, one can see the increase of crystallinity moving from sample MOF-801-1 to sample MOF-801-4 (Fig. S3). Indeed, we observed a gradual increase in the intensity of the reflections in the entire 2θ range of the experimental patterns. Full profile analysis has been performed to quantify the observed effect for the patterns shown in Fig. 6a.

The microstrains ε were fixed as $1 \cdot 10^{-6}$ to get a more precise quantitative comparison of the averaged crystalline size for this kit of samples (Table 3). We have not observed any apparent trends for the lattice parameter *a*, while a clear trend in averaged crystalline size < D > is confirmed, declaring two times larger averaged particle for the last sample in the sequence with respect to the first one. We suppose that two factors could affect the properties of material during solvent recycling. The first one could be attributed to the increase of precursors concentration in the reaction mixture. The yield of the reaction is less than 100%; therefore, unreacted molecules of fumaric acid, as well as zirconium tetrachloride, stay in DMF after synthesis. If we use the same solvent secondly, in fact, we already have a small amount of precursors in it. Therefore, after dissolving a new portion of precursors, we will obtain a solution with higher concentration. The second point is nuclei, which could not be separated by centrifugation due to the small size. As we showed previously, the first stage of UiO-66 formation is tiny tetragonal zirconium oxide particles, which are formed as a product of interaction zirconium tetrachloride with water [43]. The same process is expected during MOF-801 synthesis. So after each recycling step, we use DMF boosted with some precursors and nuclei for crystal growth.

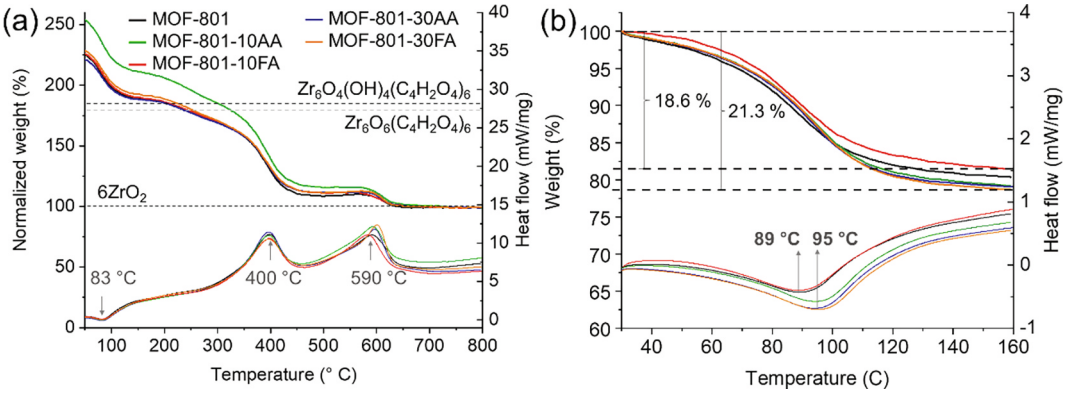

Fig. 3. TGA and DSC curves of synthesized MOF-801 samples measured in airflow (a) and N_2 (b). TGA plots in part (a) were renormalized, referring to the remaining weight at high temperature ($6ZrO_2$) as 100%. Black dotted lines in part (a) represent the normalized weight of the hydrated sample according to formula $Zr_6O_4(OH)_4(C_4O_4H_2)_6$, while gray line – dehydrated one with formula $Zr_6O_6(C_4O_4H_2)_6$. Part (b) represents accurate data in the temperature range 25–160 °C for synthesized samples treated in the same way (see details in the text).

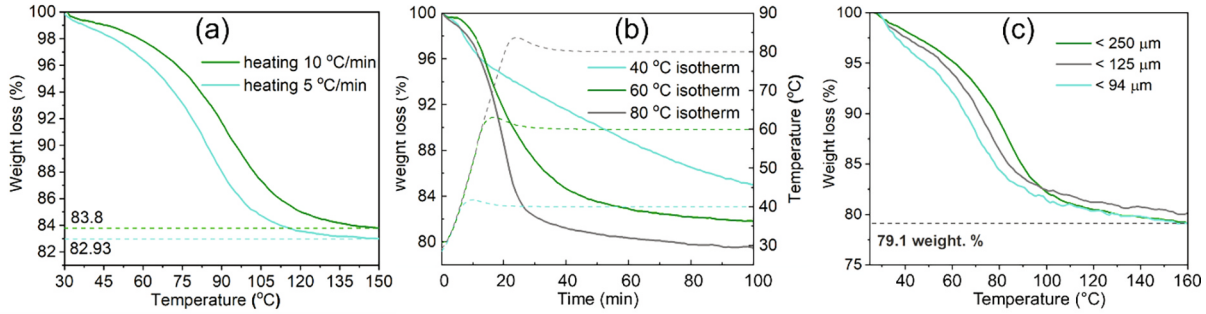

Fig. 4. TGA curves obtained for MOF-801 (10AA) sample with a different heating rate (a), and TGA isotherms measured at 40 °C, 60 °C and 80 °C (b). Part (c) represents TGA curves os sample MOF-801 with different grain sizes.

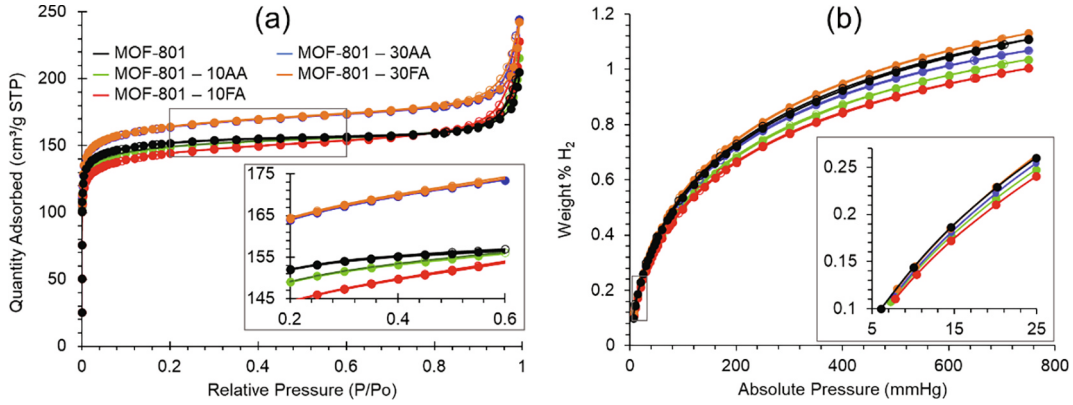

Fig. 5. Nitrogen (a) and hydrogen (b) adsorption–desorption isotherms of obtained MOF-801 samples. Filled markers showed adsorption branches of isotherms, while empty markers designate desorption ones. Inset in part (a) represents a magnification of the isotherms in region P/P_0 0.2–0.6. Inset in part (b) shows a magnification of the low-pressure region of hydrogen adsorption isotherms.

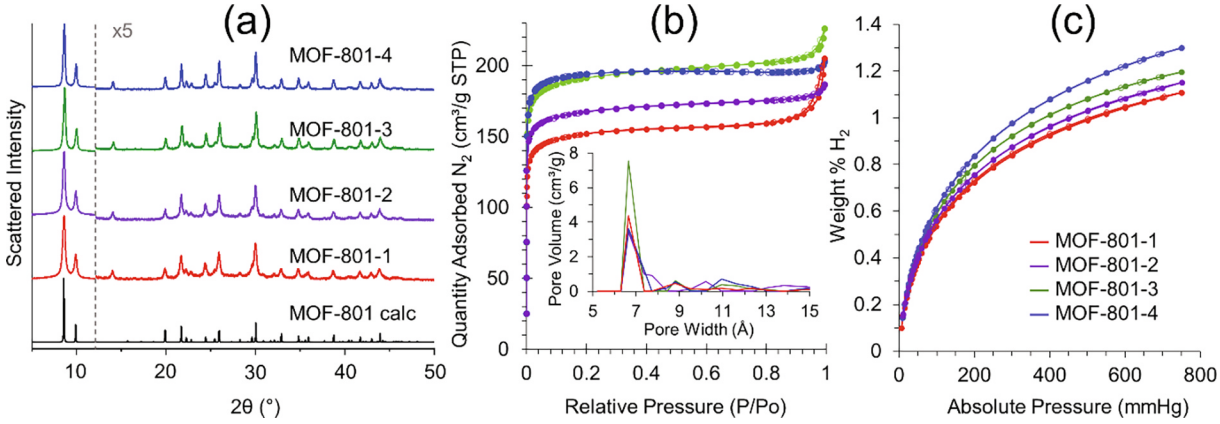

Fig. 6. (a) Powder XRD patterns of MOF-801-samples synthesized in recycled DMF. Patterns are shifted along the intensity-axis, and intensities were multiplied after the dashed line for better representation. Profile MOF-801 calc was calculated according to crystallographic data [13]. Nitrogen (b) and hydrogen (c) adsorption–desorption isotherms of MOF-801 samples obtained with recycled DMF. Filled markers show adsorption branches of isotherms, while empty markers designate desorption ones. Inset in part (b) represents pore size distribution calculated according to the Tarazona NLDFT model for cylindrical Pores.

Table 3
Some properties of samples, which were obtained in the recycling experiment. SSA stands for specific surface area. < D > designates the size of crystals calculated according to XRD data.

Sample name	Profile analysis			SSA, m^2/g	Pore volume, cm^3/g	H_2 capacity, wt.%	
	a, (Å)	< D > , (nm)	GoF, (%)			20 mmHg	750 mmHg
MOF801-1	17.914	30.52	1.23	595	0.27	0.228	1.108
MOF801-2	17.899	33.96	1.37	658	0.28	0.240	1.150
MOF801-3	17.900	44.88	1.22	749	0.33	0.242	1.197
MOF801-4	17.898	60.02	1.21	772	0.31	0.251	1.300

We also examined the evolution of such important properties like porosity and hydrogen capacity during the recycling experiment. Fig. 6b represents the nitrogen adsorption isotherms. All samples demonstrate the identical shape of isotherms, which could be assigned to type I according to IUPAC classification. It indicates that during the four cycles of the experiment, we obtained microporous materials. Specific surface areas were calculated according to the BET model (Table 3). These values exhibit a well-pronounced trend: each next step of recycling leads to the more porous material. The same trend could be observed for hydrogen capacities (Table 3, Fig. 6c). We suppose that higher crystallinity of samples leads to less-defect materials. As could be observed from pore size distribution (Fig. 6b inset), most of the cages are about 7 Å, which is close to the theoretical value (7.4 Å for octahedral cages). The crystal structure of MOF-801 with small pores is optimal for hydrogen storage. Defects, in this way, will reduce the active surface for hydrogen adsorption. Therefore, less-defect MOF-801 samples obtained in recycled DMF exhibited higher H_2 capacity.

4. Conclusions

In the present work, we have tested new fast synthesis, which is appropriate for MOF-801 large-scale production. Acetic and formic acids in two concentrations were used as modulators. We traced the effect of these modulators on the crystallinity of the product, the morphology of particles, and the porosity of the material. Moreover, such important for practical application properties as hydrogen and water capacity were investigated as well. We showed that modulator additives increase crystallinity and specific surface area of MOF-801. However, for hydrogen and water capacities, this effect is not significant, and MOF-801 could be obtained even without any additives according to suggested conditions. It allowed us to apply the recycling of the DMF. We showed that at least four times, one could obtain MOF-801 in the same solvent without any degradation of the obtained material. Moreover, the properties of MOF-801 were enhanced during recycling. We also showed that such properties as grain size, rate, and temperature of heating are crucial for successful water desorption. Recycling options and simple, fast synthesis procedure could be important for large-scale production of MOF-801.

CRediT authorship contribution statement

Vera V. Butova: Conceptualization, Writing - original draft. **Ilia A. Pankin:** Methodology, Formal analysis, Writing - original draft. **Olga A. Burachevskaya:** Validation, Investigation. **Kristina S. Vetlitsyna-Novikova:** Validation, Investigation. **Alexander V. Soldatov:** Resources, Supervision, Project administration.

Declaration of Competing Interest

The authors declare that they have no known competing financial interests or personal relationships that could have appeared to influence the work reported in this paper.

Acknowledgments

The reported study was funded by RFBR according to the research project № 18-29-04053

Appendix A. Supplementary data

Supplementary data to this article can be found online at https://doi.org/10.1016/j.ica.2020.120025.

References

[1] V.V. Butova, M.A. Soldatov, A.A. Guda, K.A. Lomachenko, C. Lamberti, Metal-organic frameworks: Structure, properties, methods of synthesis and characterization, Russ. Chem. Rev. 85 (3) (2016) 280–307.
[2] D.J. Tranchemontagne, J.L. Mendoza-Cortes, M. O'Keeffe, O.M. Yaghi, Secondary building units, nets and bonding in the chemistry of metal-organic frameworks, Chem. Soc. Rev. 38 (5) (2009) 1257–1283.
[3] V.V. Butova, V.A. Polyakov, E.A. Bulanova, M.A. Soldatov, I.S. Yahia, H.Y. Zahran, A.F. Abd El-Rehim, H. Algarni, A.M. Aboraia, A.V. Soldatov, MW synthesis of ZIF-65 with a hierarchical porous structure, Microporous Mesoporous Mat. 293 (2020).
[4] A.L. Bugaev, A.A. Guda, K.A. Lomachenko, E.G. Kamyshova, M.A. Soldatov, G. Kaur, S. Oien-Odegaard, L. Braglia, A. Lazzarini, M. Manzoli, S. Bordiga, U. Olsbye, K.P. Lillerud, A.V. Soldatov, C. Lamberti, Operando study of palladium nanoparticles inside UiO-67 MOF for catalytic hydrogenation of hydrocarbons, Faraday Discuss. 208 (2018) 287–306.
[5] S. Smolders, K.A. Lomachenko, B. Bueken, A. Struyf, A.L. Bugaev, C. Atzori, N. Stock, C. Lamberti, M.B.J. Roeffaers, D.E. De Vos, Unravelling the redox-catalytic behavior of Ce4+ metal-organic frameworks by X-ray absorption spectroscopy, ChemPhysChem 19 (4) (2018) 373–378.
[6] V.V. Butova, V.A. Polyakov, A.P. Budnyk, A.M. Aboraia, E.A. Bulanova, A.A. Guda, E.A. Reshetnikova, Y.S. Podkovyrina, C. Lamberti, A.V. Soldatov, Zn/Co ZIF family: MW synthesis, characterization and stability upon halogen sorption, Polyhedron 154 (2018) 457–464.
[7] V.V. Butova, V.A. Polyakov, E.A. Erofeeva, I.S. Yahia, H.Y. Zahran, A.F. Abd El-Rehim, A.M. Aboraia, A.V. Soldatov, Modification of ZIF-8 with triethylamine molecules for enhanced iodine and bromine adsorption, Inorg. Chim. Acta 509 (2020).
[8] H.Z. He, L.H. Du, H.L. Guo, Y.C. An, L.J. Lu, Y.L. Chen, Y. Wang, H.H. Zhong, J. Shen, J. Wu, X.T. Shuai, Redox responsive metal organic framework nanoparticles induces ferroptosis for cancer therapy, Small (2020) 11.
[9] S.A. Noorian, N. Hemmatinejad, J.A.R. Navarro, Bioactive molecule encapsulation on metal-organic framework via simple mechanochemical method for controlled topical drug delivery systems, Microporous Mesoporous Mat. 302 (2020) 8.
[10] A. Schaate, P. Roy, A. Godt, J. Lippke, F. Waltz, M. Wiebcke, P. Behrens, Modulated synthesis of Zr-based metal-organic frameworks: from nano to single crystals, Chem.-Eur. J. 17 (24) (2011) 6643–6651.
[11] L.Z. Xia, F.L. Wang, Prediction of hydrogen storage properties of Zr-based MOFs, Inorg. Chim. Acta 444 (2016) 186–192.
[12] K.S. Vetlitsyna-Novikova, V.V. Butova, I.A. Pankin, V.V. Shapovalov, A.V. Soldatov, Zirconium-based metal-organic UiO-66, UiO-66-NDC and MOF-801 frameworks. Influence of the linker effect on the hydrogen sorption efficiency, J. Surf. Ingestig. 13 (5) (2019) 787–792.
[13] H. Furukawa, F. Gandara, Y.B. Zhang, J.C. Jiang, W.L. Queen, M.R. Hudson, O.M. Yaghi, Water adsorption in porous metal-organic frameworks and related materials, J. Am. Chem. Soc. 136 (11) (2014) 4369–4381.
[14] H. Kim, H.J. Cho, S. Narayanan, S. Yang, H. Furukawa, S. Schiffres, X.S. Li, Y.B. Zhang, J.C. Jiang, O.M. Yaghi, E.N. Wang, Characterization of adsorption enthalpy of novel water-stable zeolites and metal-organic frameworks, Sci Rep 6 (2016) 8.
[15] H. Kim, S. Yang, S.R. Rao, S. Narayanan, E.A. Kapustin, H. Furukawa, A.S. Umans, O.M. Yaghi, E.N. Wang, Water harvesting from air with metal-organic frameworks powered by natural sunlight, Science 356 (6336) (2017) 430–432.
[16] H. Kim, S.R. Rao, E.A. Kapustin, L. Zhao, S. Yang, O.M. Yaghi, E.N. Wang, Adsorption-based atmospheric water harvesting device for arid climates, Nat. Commun. 9 (2018) 8.
[17] J. Choi, L.C. Lin, J.C. Grossman, Role of structural defects in the water adsorption properties of MOF-801, J. Phys. Chem. C 122 (10) (2018) 5545–5552.
[18] M.V. Solovyeva, L.G. Gordeeva, T.A. Krieger, Y.I. Aristov, MOF-801 as a promising material for adsorption cooling: Equilibrium and dynamics of water adsorption, Energy Conv. Manag. 174 (2018) 356–363.
[19] F. Ke, C.Y. Peng, T. Zhang, M.R. Zhang, C.Y. Zhou, H.M. Cai, J.F. Zhu, X.C. Wan, Fumarate-based metal-organic frameworks as a new platform for highly selective removal of fluoride from brick tea, Sci. Rep. 8 (2018) 11.
[20] X.H. Zhu, C.X. Yang, X.P. Yan, Metal-organic framework-801 for efficient removal of fluoride from water, Microporous Mesoporous Mat. 259 (2018) 163–170.
[21] T.L. Tan, P.A.P. Krusnamurthy, H. Nakajima, S.A. Rashid, Adsorptive, kinetics and regeneration studies of fluoride removal from water using zirconium-based metal organic frameworks, RSC Adv. 10 (32) (2020) 18740–18752.
[22] S.M. Prabhu, S. Kancharla, C.M. Park, K. Sasaki, Synthesis of modulator- driven highly stable zirconium- fumarate frameworks and mechanistic investigations of their arsenite and arsenate adsorption from aqueous solutions plus Phi, Crystengcomm 21 (14) (2019) 2320–2332.
[23] J. Yoo, U. Ryu, W. Kwon, K.M. Choi, A multi-dye containing MOF for the ratiometric detection and simultaneous removal of Cr2O72- in the presence of interfering ions, Sens. Actuator B-Chem. 283 (2019) 426–433.
[24] M.Q. Zheng, X.D. Zhao, K.K. Wang, Y.B. She, Z.Q. Gao, Highly efficient removal of Cr(VI) on a stable metal-organic framework based on enhanced H-bond interaction, Ind. Eng. Chem. Res. 58 (51) (2019) 23330–23337.
[25] G. Zahn, H.A. Schulze, J. Lippke, S. Konig, U. Sazama, M. Froba, P. Behrens, A water-born Zr-based porous coordination polymer: Modulated synthesis of Zr-fumarate MOF, Microporous Mesoporous Mat. 203 (2015) 186–194.
[26] W.C. Yun, M.T. Yang, K.Y.A. Lin, Water-born zirconium-based metal organic frameworks as green and effective catalysts for catalytic transfer hydrogenation of levulinic acid to gamma-valerolactone: Critical roles of modulators, J. Colloid

Interface Sci. 543 (2019) 52–63.
[27] M. Ganesh, P. Hemalatha, M.M. Peng, W.S. Cha, H.T. Jang, Zr-Fumarate MOF a Novel CO2-adsorbing material: synthesis and characterization, Aerosol Air Qual. Res. 14 (6) (2014) 1605–1612.
[28] Q.Q. Li, Q. Liu, J. Zhao, Y.Y. Hua, J.J. Sun, J.G. Duan, W.Q. Jin, High efficient water/ethanol separation by a mixed matrix membrane incorporating MOF filler with high water adsorption capacity, J. Membr. Sci. 544 (2017) 68–78.
[29] J. Zhang, H.J. Bai, Q. Ren, H.B. Luo, X.M. Ren, Z.F. Tian, S.F. Lu, Extra water- and acid-stable MOF-801 with high proton conductivity and its composite membrane for proton-exchange membrane, ACS Appl. Mater. Interfaces 10 (34) (2018) 28656–28663.
[30] C.J. Huang, Y.X. Ye, L.W. Zhao, Y.S. Li, J.L. Gu, One-pot trapping luminescent rhodamine 110 into the cage of MOF-801 for nitrite detection in aqueous solution, J. Inorg. Organomet. Polym. Mater. 29 (5) (2019) 1476–1484.
[31] N.V. Maksimchuk, J.S. Lee, M.V. Solovyeva, K.H. Cho, A.N. Shmakov, Y.A. Chesalov, J.S. Chang, O.A. Kholdeeva, Protons make possible heterolytic activation of hydrogen peroxide over Zr-based metal-organic frameworks, ACS Catal. 9 (11) (2019) 9699–9704.
[32] L. Lutterotti, R. Ceccato, R. Dal Maschio, E. Pagani, Quantitative analysis of silicate glass in ceramic materials by the Rietveld method, in: R. Delhez, E.J. Mittemeijer (Eds.), Epdic 5, Pts 1 and 2, Transtec Publications Ltd, Zurich-Uetikon, 1998, pp. 87–92.
[33] L. Lutterotti, S. Gialanella, X-ray diffraction characterization of heavily deformed metallic specimens, Acta Mater. 46 (1) (1998) 101–110.
[34] B.H. Toby, R factors in Rietveld analysis: How good is good enough? Powder Diffr. 21 (1) (2006) 67–70.
[35] V.V. Butova, K.S. Vetlitsyna-Novikova, I.A. Pankin, K.M. Charykov, A.L. Trigub, A.V. Soldatov, Microwave synthesis and phase transition in UiO-66/MIL-140A system, Microporous Mesoporous Mat. 296 (2020).
[36] S. Lopes, L. Lapinski, R. Fausto, Molecular structure and infrared spectra of dimethyl fumarate, Phys. Chem. Chem. Phys. 4 (16) (2002) 3965–3974.
[37] V.V. Butova, O.A. Burachevskaya, I.V. Ozhogin, G.S. Borodkin, A.G. Starikov, S. Bordiga, A. Damin, K.P. Lillerud, A.V. Soldatov, UiO-66 type MOFs with mixed-linkers - 1,4-Benzenedicarboxylate and 1,4-naphthalenedicarboxylate: Effect of the modulator and post-synthetic exchange, Microporous Mesoporous Mat. 305 (2020).
[38] V.V. Butova, A.P. Budnyk, A.A. Guda, K.A. Lomachenko, A.L. Bugaev, A.V. Soldatov, S.M. Chavan, S. Øien-ØDegaard, U. Olsbye, K.P. Lillerud, C. Atzori, S. Bordiga, C. Lamberti, Modulator effect in UiO-66-NDC (1, 4-naphthalenedicarboxylic acid) synthesis and comparison with UiO-67-NDC isoreticular metal-organic frameworks, Cryst. Growth Des. 17 (10) (2017).
[39] C. Atzori, G.C. Shearer, L. Maschio, B. Civalleri, F. Bonino, C. Lamberti, S. Svelle, K.P. Lillerud, S. Bordiga, Effect of benzoic acid as a modulator in the structure of UiO-66: An experimental and computational study, J. Phys. Chem. C 121 (17) (2017) 9312–9324.
[40] L. Valenzano, B. Civalleri, S. Chavan, S. Bordiga, M.H. Nilsen, S. Jakobsen, K.P. Lillerud, C. Lamberti, Disclosing the complex structure of UiO-66 metal organic framework: A synergic combination of experiment and theory, Chem. Mat. 23 (7) (2011) 1700–1718.
[41] Z. Wang, Y. Fu, Z. Kang, X. Liu, N. Chen, Q. Wang, Y. Tu, L. Wang, S. Song, D. Ling, H. Song, X. Kong, C. Fan, Organelle-specific triggered release of immunostimulatory oligonucleotides from intrinsically coordinated DNA-metal-organic frameworks with soluble exoskeleton, J. Am. Chem. Soc. 139 (44) (2017) 15784–15791.
[42] F. Fathieh, M.J. Kalmutzki, E.A. Kapustin, P.J. Waller, J.J. Yang, O.M. Yaghi, Practical water production from desert air, Sci. Adv. 4 (6) (2018) 9.
[43] V.V. Butova, A.P. Budnyk, K.M. Charykov, K.S. Vetlitsyna-Novikova, C. Lamberti, A.V. Soldatov, Water as a structure-driving agent between the UiO-66 and MIL-140A metal-organic frameworks, Chem. Commun. 55 (7) (2019) 901–904.